ORIGINAL PAPER

Nagoya J. Med. Sci. **83**. 135–149, 2021
doi:10.18999/nagjms.83.1.135

# Unenhanced CT texture analysis with machine learning for differentiating between nasopharyngeal cancer and nasopharyngeal malignant lymphoma

Hayato Tomita[1,2], Tsuneo Yamashiro[1], Gyo Iida[1], Maho Tsubakimoto[1], Hidefumi Mimura[2] and Sadayuki Murayama[1]

[1]*Department of Radiology, Graduate School of Medical Science, University of the Ryukyus, Nishihara, Japan*
[2]*Department of Radiology, St. Marianna University School of Medicine, Kawasaki, Japan*

## ABSTRACT

Differentiating between nasopharyngeal cancer and nasopharyngeal malignant lymphoma (ML) remains challenging on cross-sectional images. The aim of this study is to investigate the usefulness of texture features on unenhanced CT for differentiating between nasopharyngeal cancer and nasopharyngeal ML. Thirty patients with nasopharyngeal tumors, including 17 nasopharyngeal cancers and 13 nasopharyngeal MLs, were underwent $^{18}$F-FDG PET/CT. All nasopharyngeal cancers and 7 of 13 nasopharyngeal MLs were confirmed by endoscopic biopsy. On unenhanced CT, 34 texture features were analyzed following lesion segmentation in the maximum area of the target lesion. The Mann-Whitney U test and areas under the curve (AUCs) were used for analysis and to compare the maximum standardized uptake values (SUV) max, SUVmean, and 34 texture features. A support vector machine (SVM) was constructed to evaluate the diagnostic accuracy and AUCs of combinations of texture features, with 50 repetitions of 5-fold cross-validation. Differences between the SUVmax and SUVmean for nasopharyngeal cancers and nasopharyngeal MLs were not significant. Significant differences of texture features were seen, as follows: 1 histogram feature ($p$ = 0.038), 3 gray-level co-occurrence matrix features ($p < 0.05$), and 1 neighborhood gray-level different matrix feature (NGLDM) ($p$ = 0.003). Coarseness in NGLDM provided the highest diagnostic accuracy and largest AUC of 76.7% and 0.82, respectively. SVM evaluation of the combined texture features obtained the highest accuracy of 81.3%, with an AUC of 0.80. Combined texture features can provide useful information for discriminating between nasopharyngeal cancer and nasopharyngeal ML on unenhanced CT.

Keywords: Texture analysis, machine learning, nasopharyngeal cancer, malignant lymphoma, PET

Abbreviations:
ML: malignant lymphoma
CT : computed tomography
18F-FDG PET: fluorine-18-2-fluoro-2-deoxy-D-glucose positron emission tomography
SUV: standardized uptake value
ROI: region of interest
AUC: area under the curve
SVM: support vector machine
RFE: recursive feature elimination
GLCM: gray-level co-occurrence matrix features

Received: July 6, 2020; accepted: August 31, 2020
Corresponding Author: Hayato Tomita, MD, PhD
Department of Radiology, Graduate School of Medical Science, University of the Ryukyus,
207 Uehara, Nishihara, Okinawa 903-0215, Japan
Tel: +81-98-895-1162, E-mail: hayato.tomita@marianna-u.ac.jp

NGLDM: neighborhood gray-level different matrix



## INTRODUCTION

Nasopharyngeal cancer and nasopharyngeal malignant lymphoma (ML) are common malignant diseases of the nasopharynx that should be distinguished, because they require different treatments.[1] Although examination of endoscopic biopsy and cytology specimens is the gold standard for definitive diagnosis, such a diagnostic approach is difficult, particularly for submucosal ML lesions in the nasopharynx.[2-5] The histopathological and immunohistochemical diagnosis of ML subtypes requires an adequate amount of tissue, which must be obtained by an invasive procedure and can lead to complications, such as bleeding. Therefore, a noninvasive approach for diagnosing nasopharyngeal tumors needs to be developed.

When a nasopharyngeal tumor is suspected, computed tomography (CT) is used to evaluate the spread of head and neck tumors, cervical lymphadenopathy, and distant metastases. However, differentiating between nasopharyngeal cancer and nasopharyngeal ML remains challenging on CT, because the imaging findings of ML in the nasopharynx and nasopharyngeal carcinoma are very similar, including such findings as infiltration into the base of the skull and enlarged cervical lymph nodes with or without necrosis.[6] In addition, contrast-enhanced CT cannot be performed in some patients with nasopharyngeal tumors due to impaired renal function.

With the growing utility of artificial intelligence, various methods of quantitative analysis have become attractive because of their reproducibility and versatility. Texture analysis is a useful method for quantifying the intensity and patterns of images that cannot be recognized visually. Texture analysis studies have shown improved diagnostic characteristics, including predictive values on outcome.[7-10] However, to the best of our knowledge, texture analysis of unenhanced CT scans has not been evaluated for discrimination between nasopharyngeal cancer and nasopharyngeal ML.

The aim of this study was to clarify the usefulness of texture analysis for discriminating between nasopharyngeal cancer and nasopharyngeal ML on unenhanced CT scans.

## MATERIALS AND METHODS

This retrospective study was approved by our institutional review board, which waived the need for informed consent from patients.

*Subjects*

We initially identified 31 patients with histopathologically proven nasopharyngeal carcinoma (n=17) and nasopharyngeal ML (n=14) who underwent fluorine-18-2-fluoro-2-deoxy-D-glucose positron emission tomography ($^{18}$F-FDG PET)/CT from April 2013 to April 2018. Every patient with nasopharyngeal cancer and 7 of 14 patients with ML were confirmed on an endoscopic biopsy specimen to have a nasopharyngeal tumor. To avoid lesions that were false-positive for nasopharyngeal ML, the nasopharyngeal ML masses of the remaining 7 patients were clinically diagnosed as nasopharyngeal ML based on the following reasons: (i) thickening or mass in the nasopharynx with $^{18}$F-FDG uptake on $^{18}$F-FDG PET/CT; (ii) ML was confirmed by biopsy of enlarged lymph nodes; (iii) After treatment, reduced thickening or mass in the nasopharynx was

identified by CT, magnetic resonance imaging, or $^{18}$F-FDG PET/CT. One patient with ML who showed increased $^{18}$F-FDG uptake but did not have a detectable mass in the nasopharynx on a plain CT scan was excluded. Reviews of the imaging results were performed by 2 radiologists (*blinded and *blinded, with 8 and 19 years of experience in radiology, respectively)) who reached a consensus. Finally, a total of 30 participants were included in this study.

*FDG-PET/CT scanning*

Whole body $^{18}$F-FDG-PET examinations with CT (Biograph mCT-S(64)4R; Siemens Healthineers, Forchheim, Germany) were performed from the vertex of the skull to the pelvic floor. $^{18}$F-FDG (3.7 MBq/kg BW, max 340 MBq) was injected intravenously after at least 5 hours of fasting. Scans were obtained 1 hour later. The scanning parameters of non-contrast 64-row whole-body PET/CT scanner were as follows: tube voltage, 120 kVp; tube current, automatic exposure control (CARE Dose 4D); gantry rotation time, 0.5 sec; beam pitch, 1.5; imaging field of view, 500x500 mm; matrix, 512x512; slice thickness, 2 mm. All images were reconstructed with a B31f kernel. PET data were reconstructed using a three-dimensional iterative ordered subset expectation-maximization (OSEM) algorithm (2 iterations, 21 subsets).

*Analysis of $^{18}$F-FDG PET scans*

A commercially available workstation (Syngo via VB10; Siemens Healthineers) was used to measure the maximum standardized uptake values (SUVs) (SUVmax - maximum SUV within the region of interest [ROI]), and mean SUVs (SUVmean = mean SUV within the ROI). Uptake of FDG within the ROI, which was located to include the entire nasopharyngeal tumor was evaluated automatically on the workstation.

*Image segmentation and texture analysis on CT scans*

Texture features were analyzed in the maximum area of a target lesion on an axial image. ROI was manually drawn slightly inside the largest area of the nasopharyngeal tumor by LifeX Software (https://www.lifexsoft.com, CEA, Saclay, France) while avoiding metal artifacts.[11] When the boundary between a nasopharyngeal tumor and soft tissue was indistinct, the boundary of the tumor was contoured with reference to abnormal uptake of FDG, according to a consensus reached by 2 radiologists (*blinded and *blinded). The texture features extracted for each area were as follows: 4 histogram features, 6 gray-level co-occurrence matrix (GLCM) features, 11 gray-level run-length matrix features, 2 neighborhood gray-level different-matrix (NGLDM) features, 11 gray-level zone-length matrix features. The list of all texture features is provided in Appendix 1.

*Statistical analysis*

Statistical analysis is performed using JMP 10.0.2 software (SAS Institute, Cary, NC, USA). Data were expressed as means ± standard deviation. Comparisons between the SUVmax, SUVmean, and 34 texture features of the ROIs of nasopharyngeal cancers and nasopharyngeal MLs were evaluated by the Mann-Whitney U test. Receiver operating characteristic (ROC) curves were constructed, and the area under the curve (AUC) of each ROC was measured for each texture feature. A python-based support vector machine (SVM) with radial basis kernel in the machine learning library 'scikit-learn' (v0.16.1; http://scikit-learn.org) was implemented to evaluate the performance of combined texture features, with 50 repetitions of 5-fold cross validation. In 5-fold cross validation, the data are split into 5 folds. The first fold is used to test the model and the rest are used to train the model. The 5-fold cross-validation procedure was repeated 50 times with different splits in each repetition, in order to avoid split bias.[12] The mean

score of each fold used for testing was calculated to evaluate the performance of the model. The grid search method was used to select the optimized SVM parameters, C and gamma. The best combinations of texture features were selected by recursive feature elimination (RFE). RFE reduced the combination of texture features to a specified number of texture features, based on importance.[13] All $p$-values < 0.05 were considered significant.

## RESULTS

The characteristics of patients and tumors are summarized in Table 1. The most common histopathological type of the nasopharyngeal cancers and MLs were poorly differentiated squamous cell carcinoma and diffuse large B-cell lymphoma, respectively. The CT-related radiation dose to the patient was calculated from the computed tomography dose index (CTDI). The mean CTDI was 4.48±1.48 mGy.

*Comparisons of the SUVmax and SUVmean between the nasopharyngeal cancers and nasopharyngeal MLs*

The SUVmax and SUVmean of the nasopharyngeal cancers and nasopharyngeal MLs are shown in Table 2. The differences of the SUVmax and SUVmean between the nasopharyngeal cancers and nasopharyngeal MLs were not significant.

*Comparisons of the texture features between the nasopharyngeal cancers and nasopharyngeal MLs*

Appendix 2 shows the measurements of 34 texture features on unenhanced CT scans. Correlations between tumor voxel and texture features are shown in Appendix 3. Texture features with strong correlation (correlation coefficient >0.7) with tumor voxel were excluded to avoid the effect of confounding factors.[14]

**Table 1** Characteristics of patients and tumors (nasopharyngeal carcinomas and malignant lymphomas)

| | **Nasopharyngeal carcinoma** | | **Nasopharyngeal ML** | |
|---|---|---|---|---|
| **Age mean ± SD** | 52.3 ± 7.8 | | 68.8 ± 7.1 | |
| **male/female** | 4/13 | | 6/7 | |
| **Histological types** | Poorly differentiated SCC | 6 | Diffuse large B-cell lymphoma | 11 |
| | Moderate differentiated SCC | 2 | Intravenous lymphoma | 1 |
| | Nonkeratinizing differentiated SCC | 2 | Adult T-cell lymphoma | 1 |
| | Nonkeratinizing undifferentiated SCC | 1 | | |
| | Lymphoepithelial carcinoma | 2 | | |
| | Poorly differentiated adenocarcinoma | 1 | | |
| | Undefined | 3 | | |
| **T stage/Clinical stage** | T1 | 1 | I | 2 |
| | T2 | 9 | II | 4 |
| | T3 | 3 | III | 0 |
| | T4 | 4 | IV | 7 |

ML: malignant lymphoma
SD: standard deviation
SCC: squamous cell carcinoma

The differences between nasopharyngeal cancers and nasopharyngeal MLs were significant for energy in histogram ($p$ = 0.038); energy, correlation, and entropy in GLCM ($p$ = 0.017, $p$ = 0.042, and $p$ = 0.013, respectively); and coarseness in NGLDM ($p$ = 0.003). Table 3 summarizes the measurements of selected texture features. Coarseness in NGLDM provided the highest accuracy and largest AUC of 76.7% and 0.82, respectively, with a sensitivity of 64.7% and specificity of 92.3%.

The combination of 5 texture features (coarseness in NGLDM, entropy in GLCM, energy in GLCM, correlation in GLCM, and energy in Histogram) showed the highest accuracy of 81.3%, with a sensitivity of 81.9%, a specificity of 66.7%, and an AUC of 0.80. Figures 1 and 2 show representative cases for the differentiation between nasopharyngeal cancer and nasopharyngeal ML by SVM evaluation using the combination of texture features.

**Table 2** Comparisons between SUVmax and SUVmean of nasopharyngeal carcinomas versus nasopharyngeal malignant lymphomas

| | **Nasopharyngeal carcinoma** | **Nasopharyngeal ML** | |
|---|---|---|---|
| | Mean ± SD | Mean ± SD | $p$ |
| SUVmax | 15.20 ± 3.13 | 17.70 ± 13.17 | 0.346 |
| SUVmean | 8.62 ± 1.98 | 11.10 ± 8.07 | 0.267 |

ML: malignant lymphoma
SD: standard deviation
SUV: standardized uptake value.

**Table 3** Comparisons between selected texture features in maximum areas of nasopharyngeal carcinomas versus nasopharyngeal malignant lymphomas

| | **Nasopharyngeal carcinoma** | **Nasopharyngeal ML** | | | | | | |
|---|---|---|---|---|---|---|---|---|
| | Mean ± SD | Mean ± SD | $p$ | cut-off | SEN (%) | SPE (%) | ACC (%) | AUC |
| **Histogram** | | | | | | | | |
| Energy | 0.131 ± 0.02 | 0.144 ± 0.02 | 0.038* | 0.130 | 70.6 | 69.2 | 76.7 | 0.72 |
| **GLCM** | | | | | | | | |
| Energy | 0.019 ± 0.02 | 0.025 ± 0.01 | 0.017* | 0.026 | 100 | 46.1 | 70.0 | 0.76 |
| Correlation | 0.145 ± 0.11 | 0.087 ± 0.13 | 0.042* | 0.132 | 70.6 | 76.9 | 73.3 | 0.72 |
| Entropy | 1.841 ± 0.09 | 1.732 ± 0.173 | 0.013* | 1.720 | 100 | 46.1 | 76.7 | 0.77 |
| **NGLDM** | | | | | | | | |
| Coarseness | 0.016 ± 0.001 | 0.035 ± 0.02 | 0.003* | 0.014 | 64.7 | 92.3 | 76.7 | 0.82 |

ML: malignant lymphoma
AUC: the area under the curve
SD: standard deviation
GLCM: gray-level co-occurrence matrix
NGLDM: neighborhood grey-level different matrix
SEN: Sensitivity
SPE: Specificity
ACC: Accuracy
* indicates significant differences.


**Fig. 1** A 30-year-old man with nasopharyngeal carcinoma

**Fig.1A-1C:** Minimum intensity projection in FDG image (A) and unenhanced CT image (B) show the nasopharyngeal tumor and enlargement of right Rouvière lymph node (arrow). ROI shown in color was manually drawn (C).

Coarseness in NGLDM (0.009; cut-off value [COV] < 0.014), entropy in GLCM (1.90; COV > 1.72), energy in GLCM (0.016; COV < 0.026), correlation in GLCM (0.140; COV > 0.132), and energy in histogram (0.12; COV < 0.13), derived from the nasopharyngeal tumor revealed the true positive values while the SUVmax and SUVmean showed 12.42 and 7.03.

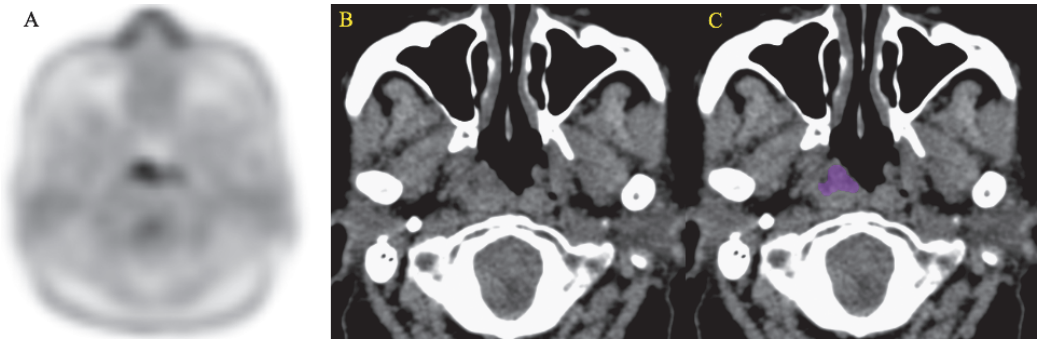


**Fig. 2** A 67-year-old woman with malignant lymphoma

**Fig. 2A-2C:** Minimum intensity projection in FDG image (A) and unenhanced CT image (B) show the nasopharyngeal tumor. ROI shown in color was manually drawn (C).

Coarseness in NGLDM (0.052; cut-off value [COV] > 0.014), energy in GLCM (0.028; COV > 0.026), correlation in GLCM (0.128; COV < 0.132), entropy in GLCM (1.64; COV < 1.72), and energy in histogram (0.15; COV > 0.13) derived from the nasopharyngeal malignant lymphoma revealed the true positive while the SUVmax and SUVmean showed 10.49 and 6.10.

## DISCUSSION

In our study, significant differences of some texture features extracted from the maximum areas of nasopharyngeal tumor on unenhanced CT scans between nasopharyngeal cancers and nasopharyngeal MLs indicate that those texture features might be able to distinguish nasopharyngeal cancer from nasopharyngeal ML. However, the SUVmax and SUVmean derived from PET/CT scans of those tumors did not differentiate between nasopharyngeal cancer and nasopharyngeal ML.

Differentiating between nasopharyngeal cancer and nasopharyngeal ML on cross-sectional

CT images is sometimes difficult, because of similarity in the findings, which include spreading pattern, necrotic tumor, and cervical lymphadenopathy. Initial whole-body $^{18}$F-FDG PET for patients with nasopharyngeal tumors prioritizes evaluating for the presence of the original lesion in the nasopharynx, locations of metastases, and lymphadenopathy. Previous reports have shown that differences between the SUVmax derived from $^{18}$F-FDG PET scans of nasopharyngeal cancer and scans of nasopharyngeal ML were not significant.[15,16] In our study, the SUVmax and SUVmean also did not differentiate between nasopharyngeal cancer and nasopharyngeal ML. Kato et al described that different histopathological types of nasopharyngeal ML can affect glucose metabolism, which might partially account for the inability of $^{18}$F-FDG PET to distinguish nasopharyngeal cancer from nasopharyngeal ML.[16]

In our study, texture analysis of unenhanced CT scans from $^{18}$F-FDG PET/CT examinations provided useful information for distinguishing nasopharyngeal cancer from nasopharyngeal ML. Texture analysis reveals the spatial distributions and relationships of gray-level patterns in target lesions. CT, magnetic resonance imaging, and PET have previously been used to obtain the characteristics of tissues within tumors, such as heterogeneity, uniformity, and granularity.[17-19] Heterogeneity in malignant lesions are recognized to be associated with disorders of attenuation due to increased cellularity, necrosis, and angiogenesis.[20] Overlapping imaging findings between nasopharyngeal cancers and nasopharyngeal ML have been observed, since they both have lesions showing homogeneity and necrosis.[21] However, in our study, entropy in GLCM related to the randomness of gray levels was higher in nasopharyngeal cancer than in nasopharyngeal ML, while energy in histogram and GLCM related to uniformity and coarseness in NGLDM related to homogeneity were lower. Therefore, texture analysis might be able to discriminate between small differences in grey levels that cannot be evaluated visually.

Texture analysis of unenhanced CT scans obtained with low radiation doses appears to be of increasing interest. CT scans with $^{18}$F-FDG PET are performed at a lower radiation dose than the dose used for conventional diagnostic CT scans that focus on identifying the location of lesions and the anatomical structures of the whole body. Previous studies have demonstrated the usefulness of PET/CT performed with low-dose unenhanced CT for the staging of ML.[22,23] The CTDI in our study was 4.48 mGy, which was a lower radiation dose than the CTDIs reported in previous studies.[24,25] CT performed with a reduced radiation dose results in increased image noise. However, Buch et al performed a phantom study that indicated that tube current did not affect texture analysis.[26] Texture features extracted from CT images obtained with a low radiation dose should also be sensitive to changes in gray-level patterns in nasopharyngeal tumors.

This study has limitations. First, some nasopharyngeal MLs were not confirmed in biopsy specimens from the nasopharynx. Previous reports demonstrated that incidental nasopharyngeal uptake of $^{18}$F-FDG was seen in 4.9%–5.2% of all $^{18}$F-FDG PET examinations.[27,28] Lee et al demonstrated that the SUVmax (range 1.8 to 10.5; mean 3.9±1.4) of benign nasopharyngeal lesions was significantly lower than the SUVmax of nasopharyngeal cancers.[28] In our study, there was an ML patient with the SUVmax <10 in the nasopharyngeal lesion. However, the size of the tumor was found to be reduced after treatment. Second, the ROIs of tumors were manually segmented. A patient was excluded because distinguishing normal tissue from tumor tissue could not be performed on the unenhanced CT scan. It is possible that manual segmentation of target lesions might affect the texture features. Computerized automated segmentation with reference to a contrast-enhanced CT image will be required to show high reproducibility in future studies. Third, this was a retrospective study with a small number of patients. Our findings should be investigated by classifiers for validations and testing of machine learning in a larger prospective study with patients diagnosed using biopsy specimens from the nasopharynx.

In our conclusion, quantitative analysis of texture features on unenhanced CT scans should

be useful for differentiating between nasopharyngeal cancer and nasopharyngeal ML, whereas the SUVmax and SUVmean derived from PET/CT did not differentiate between the cancers.

## CONFLICTS OF INTEREST

The authors have declared no conflicts of interest.

## REFERENCES

1 Mukherji SK. Pharynx. In: Som PM, Curtin HD editors. Head and Neck Imaging. 4th ed. St. Louis, MO. *Mosby Elsevier*; 2003:1464–1520.
2 Nadjib M, Lubis D. The technical procedure and the value of fine needle aspiration biopsy of the nasopharynx. *Pathology*. 1993;25(1):35–38. doi:10.3109/00313029309068899.
3 Layfield LJ. Fine-needle aspiration in the diagnosis of head and neck lesions: a review and discussion of problems in differential diagnosis. *Diagn Cytopathol*. 2007;35(12):798–805. doi:10.1002/dc.20769.
4 Zhang ZM, Bao Y, Zhou LX, Zhao R, Huang J, Liu WS. Feasibility of Diagnosing a Submucosal Nasopharyngeal Carcinoma by Endonasopharyngeal Ultrasound-Guided Transnasopharyngeal Needle Aspiration. *Chin Med J (Engl)*. 2018;131(12):1506–1508. doi:10.4103/0366-6999.233947.
5 Scher RL, Oostingh PE, Levine PA, Cantrell RW, Feldman PS. Role of fine needle aspiration in the diagnosis of lesions of the oral cavity, oropharynx, and nasopharynx. *Cancer*. 1988;62(12):2602–2606. doi:10.1002/1097-0142(19881215)62:12<2602::aid-cncr2820621225>3.0.co;2-9.
6 Kato H, Kanematsu M, Kawaguchi S, Watanabe H, Mizuta K, Aoki M. Evaluation of imaging findings differentiating extranodal non-Hodgkin's lymphoma from squamous cell carcinoma in naso- and oropharynx. *Clin Imaging*. 2013;37(4):657–663. doi:10.1016/j.clinimag.2012.11.007.
7 Buch K, Fujita A, Li B, Kawashima Y, Qureshi MM, Sakai O. Using Texture Analysis to Determine Human Papillomavirus Status of Oropharyngeal Squamous Cell Carcinomas on CT. *AJNR Am J Neuroradiol*. 2015;36(7):1343–1348. doi:10.3174/ajnr.A4285.
8 Schieda N, Thornhill RE, Al-Subhi M, et al. Diagnosis of Sarcomatoid Renal Cell Carcinoma With CT: Evaluation by Qualitative Imaging Features and Texture Analysis. *AJR Am J Roentgenol*. 2015;204(5):1013–1023. doi:10.2214/AJR.14.13279.
9 Kuno H, Qureshi MM, Chapman MN, et al. CT Texture Analysis Potentially Predicts Local Failure in Head and Neck Squamous Cell Carcinoma Treated with Chemoradiotherapy. *AJNR Am J Neuroradiol*. 2017;38(12):2334–2340. doi:10.3174/ajnr.A5407.
10 Kirienko M, Cozzi L, Antunovic L, et al. Prediction of disease-free survival by the PET/CT radiomic signature in non-small cell lung cancer patients undergoing surgery. *Eur J Nucl Med Mol Imaging*. 2018;45(2):207–217. doi:10.1007/s00259-017-3837-7.
11 Nioche C, Orlhac F, Boughdad S, et al. LIFEx: A Freeware for Radiomic Feature Calculation in Multimodality Imaging to Accelerate Advances in the Characterization of Tumor Heterogeneity. *Cancer Res*. 2018;78(16):4786–4789. doi:10.1158/0008-5472.CAN-18-0125.
12 Krstajic D, Buturovic LJ, Leahy DE, Thomas S. Cross-validation pitfalls when selecting and assessing regression and classification models. *J Cheminform*. 2014;6(1):10. doi:10.1186/1758-2946-6-10.
13 Feng Z, Rong P, Cao P, et al. Machine learning-based quantitative texture analysis of CT images of small renal masses: Differentiation of angiomyolipoma without visible fat from renal cell carcinoma. *Eur Radiol*. 2018;28(4):1625–1633. doi:10.1007/s00330-017-5118-z.
14 Mukaka MM. Statistics corner: A guide to appropriate use of correlation coefficient in medical research. *Malawi Med J*. 2012;24(3):69–71.
15 Cho KS, Kang DW, Kim HJ, Lee JK, Roh HJ. Differential diagnosis of primary nasopharyngeal lymphoma and nasopharyngeal carcinoma focusing on CT, MRI, and PET/CT. *Otolaryngol Head Neck Surg*. 2012;146(4):574–578. doi:10.1177/0194599811434712.
16 Kato H, Kanematsu M, Watanabe H, Kawaguchi S, Mizuta K, Aoki M. Differentiation of extranodal non-Hodgkins lymphoma from squamous cell carcinoma of the maxillary sinus: a multimodality imaging approach. *Springerplus*. 2015;4:228. doi:10.1186/s40064-015-0974-y.
17 Davnall F, Yip CS, Ljungqvist G, et al. Assessment of tumor heterogeneity: an emerging imaging tool for clinical practice? *Insights Imaging*. 2012;3(6):573–589. doi:10.1007/s13244-012-0196-6.

18 Karahaliou A, Vassiou K, Arikidis NS, Skiadopoulos S, Kanavou T, Costaridou L. Assessing heterogeneity of lesion enhancement kinetics in dynamic contrast-enhanced MRI for breast cancer diagnosis. *Br J Radiol*. 2010;83(988):296–309. doi:10.1259/bjr/50743919.
19 Hyun SH, Kim HS, Choi SH, et al. Intratumoral heterogeneity of (18)F-FDG uptake predicts survival in patients with pancreatic ductal adenocarcinoma. *Eur J Nucl Med Mol Imaging*. 2016;43(8):1461–1468. doi:10.1007/s00259-016-3316-6.
20 Bayanati H, E Thornhill R, Souza CA, et al. Quantitative CT texture and shape analysis: can it differentiate benign and malignant mediastinal lymph nodes in patients with primary lung cancer?. *Eur Radiol*. 2015;25(2):480–487. doi:10.1007/s00330-014-3420-6.
21 Toma P, Granata C, Rossi A, Garaventa A. Multimodality imaging of Hodgkin disease and non-Hodgkin lymphomas in children. *Radiographics*. 2007;27(5):1335–1354. doi:10.1148/rg.275065157.
22 Schaefer NG, Hany TF, Taverna C, et al. Non-Hodgkin lymphoma and Hodgkin disease: coregistered FDG PET and CT at staging and restaging–do we need contrast-enhanced CT? *Radiology*. 2004;232(3):823–829. doi:10.1148/radiol.2323030985.
23 Raanani P, Shasha Y, Perry C, et al. Is CT scan still necessary for staging in Hodgkin and non-Hodgkin lymphoma patients in the PET/CT era? *Ann Oncol*. 2006;17(1):117–122. doi:10.1093/annonc/mdj024.
24 Shrimpton PC, Hillier MC, Lewis MA, Dunn M. National survey of doses from CT in the UK: 2003. *Br J Radiol*. 2006;79(948):968–980. doi:10.1259/bjr/93277434.
25 Bodelle B, Beeres M, Scheithauer S, et al. Automated Tube Potential Selection as a Method of Dose Reduction for CT of the Neck: First Clinical Results. *AJR Am J Roentgenol*. 2015;204(5):1049–1054. doi:10.2214/AJR.14.12975.
26 Buch K, Li B, Qureshi MM, Kuno H, Anderson SW, Sakai O. Quantitative Assessment of Variation in CT Parameters on Texture Features: Pilot Study Using a Nonanatomic Phantom. *AJNR Am J Neuroradiol*. 2017;38(5):981–985. doi:10.3174/ajnr.A5139.
27 Chen YK, Su CT, Chi KH, Cheng RH, Wang SC, Hsu CH. Utility of 18F-FDG PET/CT uptake patterns in Waldeyer's ring for differentiating benign from malignant lesions in lateral pharyngeal recess of nasopharynx. *J Nucl Med*. 2007;48(1):8–14.
28 Lee N, Yoo I, Park SY, Yoon H, Lee Y, Oh JK. Significance of Incidental Nasopharyngeal Uptake on (18) F-FDG PET/CT: Patterns of Benign/Physiologic Uptake and Differentiation from Malignancy. *Nucl Med Mol Imaging*. 2015;49(1):11–18. doi:10.1007/s13139-014-0299-8.

**Appendixes:**

**Appendix 1** Definition of texture features

1. Histogram features

Histogram features consist of simple statistics that are associated with pixel values in images, while spatial patterns of pixel values are not included. Skewness, kurtosis, entropy, and energy were calculated.

2. Gray-level co-occurrence matrix (GLCM) features

GLCM is the distribution of co-occurring pixel values that are calculated from four directions in 2-dimensional (2D) space or 13 directions in 3-dimensional (3D) space:

Homogeneity $= \sum_{i,j} \frac{p(i,j)}{1+|i-j|}$

Energy $= \sum_{i,j} p(i,j)^2$

Contrast $= \sum_{i,j} |i-j|^2 \, p(i,j)$

Correlation $= \sum_{i,j} \frac{(i-\mu_i)(j-\mu_j)p(i,j)}{\sigma_i \sigma_j}$

Entropy $= \sum_{i,j} \log(p(i,j))p(i,j)$

Dissimilarity $= \sum_{i,j} |i-j|p(i,j)$

Where *p(i,j)* represents *(i,j)* value of the GLCM.

3. Gray-level run length matrix (GLRLM) features

The GLRLM describes *the number of consecutive* pixels of the same gray-level value for four directions in 2D space or 13 directions in 3D space:

Short run emphasis (SRE) $= \frac{1}{n_r} \sum_{i,j} \frac{p(i,j)}{j^2}$

Long run emphasis (LRE) $= \frac{1}{n_r} \sum_{i,j} p(i,j) j^2$

Low gray-level run emphasis (LGRE) $= \frac{1}{n_r} \sum_{i,j} \frac{p(i,j)}{i^2}$

High gray-level run emphasis (HGRE) $= \frac{1}{n_r} \sum_{i,j} p(i,j) i^2$

Short run low gray-level emphasis (SRLGE) $= \frac{1}{n_r} \sum_{i,j} \frac{p(i,j)}{i^2 j^2}$

Short run high gray-level emphasis (SRHGE) $= \frac{1}{n_r} \sum_{i,j} \frac{p(i,j) i^2}{j^2}$

Long run low gray-level emphasis (LRLGE) $= \frac{1}{n_r} \sum_{i,j} \frac{p(i,j) j^2}{i^2}$

Long run high gray-level emphasis (LRHGE) $= \sum_{i,j} p(i,j) i^2 j^2$

Gray-level non-uniformity (GLNU) $= \frac{1}{n_r} \sum_i \left( \sum_j p(i,j) \right)^2$

Run length non-uniformity (RLNU) = $\frac{1}{n_r}\sum_j(\sum_i p(i,j))^2$

Run percentage (RP) = $\frac{n_r}{\sum_{i,j}(jp(i,j))}$

Where $n_r$ corresponds to the number of homogenous runs.

4. Neighborhood gray-level different matrix (NGLDM)

NGLDM describes the difference in gray-levels between adjacent voxels of 8 in 2D space and 26 in 3D space:

Coarseness = $\frac{1}{\sum_i p(i,1)p(i,2)}$

Contrast = $\left[\sum_{i,j} p(i,1)p(j,1)(i-j)^2\right]\frac{\sum_i p(i,2)}{EG(G-1)}$

Where E is the number of voxels in VOI and G is the number of gray-levels.

5. Gray-level zone length matrix (GLZLM)

GLZLM describes *the number of homogenous zones* of the same gray-level value in 2D or 3D space:

Short-zone emphasis (SZE) = $\frac{1}{n_r}\sum_{i,j}\frac{p(i,j)}{j^2}$

Long-zone emphasis (LZE) = $\frac{1}{n_r}\sum_{i,j} p(i,j)j^2$

Low gray-level zone emphasis (LGZE) = $\frac{1}{n_r}\sum_{i,j}\frac{p(i,j)}{i^2}$

High gray-level zone emphasis (HGZE) = $\frac{1}{n_r}\sum_{i,j} p(i,j)i^2$

Short-zone low gray-level emphasis (SZLGE) = $\frac{1}{n_r}\sum_{i,j}\frac{p(i,j)}{i^2j^2}$

Short-zone high gray-level emphasis (SZHGE) = $\frac{1}{n_r}\sum_{i,j}\frac{p(i,j)i^2}{j^2}$

Long-zone low gray-level emphasis (LZLGE) = $\frac{1}{n_r}\sum_{i,j}\frac{p(i,j)j^2}{i^2}$

Long-zone high gray-level emphasis (LZHGE) = $\frac{1}{n_r}\sum_{i,j} p(i,j)i^2j^2$

Gray-level non-uniformity for zone (GLNU) = $\frac{1}{n_r}\sum_i\left(\sum_j p(i,j)\right)^2$

Zone length non-uniformity (ZLNU) = $\frac{1}{n_r}\sum_j(\sum_i p(i,j))^2$

Zone percentage (ZP) = $\frac{n_r}{\sum_{i,j}(jp(i,j))}$

where $n_r$ corresponds to the number of homogenous zones.

**Appendix 2** Comparisons between texture features of nasopharyngeal carcinomas and nasopharyngeal malignant lymphomas

| | Nasopharyngeal carcinoma | Nasopharyngeal ML | |
|---|---|---|---|
| | Mean ± SD | Mean ± SD | *p* |
| **Histogram** | | | |
| Skewness | –0.023 ± 0.025 | 0.027 ± 0.103 | 0.818 |
| Kurtosis | 2.977 ± 0.600 | 2.924 ± 0.119 | 0.586 |
| Entropy | 0.951 ± 0.060 | 0.916 ± 0.067 | 0.176 |
| Energy | 0.131 ± 0.022 | 0.144 ± 0.020 | 0.038* |
| **GLCM** | | | |
| Homogeneity | 0.425 ± 0.022 | 0.432 ± 0.056 | 0.464 |
| Energy | 0.019 ± 0.022 | 0.025 ± 0.009 | 0.017* |
| Contrast | 8.408 ± 1.745 | 8.173 ± 4.191 | 0.722 |
| Correlation | 0.145 ± 0.111 | 0.087 ± 0.129 | 0.042* |
| Entropy | 1.841 ± 0.090 | 1.732 ± 0.173 | 0.013* |
| Dissimilarity | 2.269 ± 0.217 | 2.221 ± 0.584 | 0.660 |
| **GLRLM** | | | |
| SRE | 0.899 ± 0.008 | 0.903 ± 0.024 | 0.586 |
| LRE | 1.511 ± 0.051 | 1.495 ± 0.11 | 0.645 |
| LGRE | 9.037 ± 8.57E-12 | 9.063 ± 1.53E-12 | 1.000 |
| HGRE | 11088 ± 111 | 11054 ± 190 | 0.923 |
| SRLGE | 8.126 ± 1.29E-12 | 8.181 ± 7.44E-12 | 1.000 |
| SRHGE | 9971 ± 191 | 9977 ± 436 | 0.983 |
| LRLGE | 1.365 ± 5.59E-11 | 1.355 ± 1.22E-11 | 1.000 |
| LRHGE | 16750 ± 433 | 16526 ± 950 | 0.517 |
| GLNU | 52.65 ± 9.424 | 26.11 ± 10.790 | 0.006* |
| RLNU | 325.6 ± 30.18 | 153.6 ± 94.13 | 0.003* |
| RP | 0.868 ± 0.010 | 0.872 ± 0.025 | 0.503 |
| **NGLDM** | | | |
| Coarseness | 0.016 ± 0.001 | 0.035 ± 0.024 | 0.003* |
| Contrast | 0.101 ± 0.076 | 0.117 ± 0.029 | 0.142 |
| **GLZLM** | | | |
| SZE | 0.705 ± 0.019 | 0.706 ± 0.04 | 0.967 |
| LZE | 5.701 ± 1.129 | 5.662 ± 1.293 | 0.503 |
| LGZE | 0.904 ± 1.15E-10 | 0.9064 ± 1.67E-10 | 1.000 |
| HGZE | 11089 ± 145.4 | 11056 ± 206.3 | 0.38 |
| SZLGE | 0.638 ± 6.77E-10 | 0.6401 ± 2.10E-10 | 1.000 |
| SZHGE | 7823 ± 343.9 | 7814 ± 619.8 | 0.967 |
| LZLGE | 0.515 ± 1.05E-07 | 0.514 ± 1.27E-07 | 1.000 |
| LZHGE | 63189 ± 12166 | 62447 ± 13145 | 0.558 |
| GLNU | 29.89 ± 3.868 | 14.93 ± 7.432 | 0.004* |
| ZLNU | 125.56 ± 5.337 | 60.54 ± 46.4 | 0.003* |
| ZP | 0.562 ± 0.039 | 0.574 ± 0.063 | 0.660 |

ML: malignant lymphoma

SD: standard deviation

ML: malignant lymphoma;

GLCM: gray-level co-occurrence matrix features

GLRLM: gray-level run-length matrix features

SRE: short run emphasis
LRE: long run emphasis
LGRE: low gray-level run emphasis
HGRE: high gray-level run emphasis
SRLGE: short run low gray-level emphasis
SRHGE: short run high gray-level emphasis
LRLGE: long run low gray-level emphasis
LRHGE: long run high gray-level emphasis
GLNU: gray-level non-uniformity
RLNU: run-length non-uniformity
RP: run percentage
NGLDM: neighborhood gray-level different matrix
GLZLM: gray-level zone length matrix
SZE: short-zone emphasis
LZE: long-zone emphasis
LGZE: low gray-level zone emphasis
HGZE: high gray-level zone emphasis
SZLGE: short-zone low gray-level emphasis
SZHGE: short-zone high gray-level emphasis
LZLGE: long-zone low gray-level emphasis
LZHGE: long-zone high gray-level emphasis
ZLNU: zone-length non-uniformity
ZP: zone percentage
* indicates significant differences.

**Appendix 3** Correlations between texture features and tumor voxels

| | Correlation coefficient (r) |
|---|---|
| **Histogram** | |
| Skewness | –0.014 |
| Kurtosis | 0.191 |
| Entropy | 0.336 |
| Energy | –0.387 |
| **GLCM** | |
| Homogeneity | –0.165 |
| Energy | –0.513 |
| Contrast | 0.103 |
| Correlation | 0.184 |
| Entropy | 0.573 |
| Dissimilarity | 0.127 |
| **GLRLM** | |
| SRE | –0.110 |
| LRE | 0.096 |
| LGRE | 0 |
| HGRE | 0.387 |
| SRLGE | 0 |
| SRHGE | 0.108 |
| LRLGE | 0 |
| LRHGE | 0.164 |
| GLNU | 0.995* |
| RLNU | 0.998* |
| RP | –0.127 |
| **NGLDM** | |
| Coarseness | –0.684 |
| Contrast | –0.498 |
| **GLZLM** | |
| SZE | –0.054 |
| LZE | 0.205 |
| LGZE | 0 |
| HGZE | 0.344 |
| SZLGE | 0 |
| SZHGE | –0.004 |
| LZLGE | 0 |
| LZHGE | 0.223 |
| GLNU | 0.998* |
| ZLNU | 0.986* |
| ZP | –0.209 |

GLCM: gray-level co-occurrence matrix features
GLRLM : gray-level run-length matrix features
SRE: short run emphasis
LRE: long run emphasis
LGRE: low gray-level run emphasis
HGRE: high gray-level run emphasis
SRLGE: short run low gray-level emphasis

SRHGE: short run high gray-level emphasis
LRLGE: long run low gray-level emphasis
LRHGE: long run high gray-level emphasis
GLNU: gray-level non-uniformity
RLNU: run-length non-uniformity
RP: run percentage
NGLDM: neighborhood gray-level different matrix
GLZLM: gray-level zone length matrix
SZE: short-zone emphasis
LZE: long-zone emphasis
LGZE: low gray-level zone emphasis
HGZE: high gray-level zone emphasis
SZLGE: short-zone low gray-level emphasis
SZHGE: short-zone high gray-level emphasis
LZLGE: long-zone low gray-level emphasis;
LZHGE: long-zone high gray-level emphasis
ZLNU: zone-length non-uniformity
ZP: zone percentage.
* indicates the correlation of more than 0.7 between each texture feature and tumor volume.